Improved CIR-Based Receiver Design for DVB-T2 System in Large Delay Spread Channels: Synchronization and Equalization

Jong-Seob Baek and Jong-Soo Seo, *Member, IEEE*

***Abstract*—This paper proposes to implement an improved orthogonal frequency division multiplexing (OFDM) receiver by utilizing a channel impulse response (CIR)-based synchronization and sparse equalization for DVB-T2 system operating in both the single-input single-output (SISO) and multi-input single-output (MISO) transmission modes. First, the proposed OFDM receiver performs a pilot-aided CIR estimation after a coarse symbol timing recovery (STR). Then, the proposed CIR-based fine STR compensates for a false symbol timing offset (STO). In particular, the fine STR resolves an ambiguity effect of CIR, which is the main problem caused by a false coarse STO in exploiting the CIR. Upon the completion of the fine synchronization, the proposed CIR-based sparse equalization is performed in order to minimize the noise and interference effects by shifting or selecting a basic frequency interpolation (FI) filter according to an echo delay (phase) or maximum delay spread, respectively. Performance evaluations are accomplished in large delay spread channels in which the maximum delay spread is less or longer than a guard interval (GI). It is shown that the proposed receiver is not only capable of estimating the fine STO but also minimizing effectively the noise effects. In particular, the performance gain in a single pre-echo channel being longer than GI is remarkable as compared with a conventional receiver.**

***Index Terms*—DVB-T2, equalization, MISO, OFDM, symbol timing recovery.**

I. Introduction

IMPROVED efficient receiver design is an important practical issue for next-generation broadcast techniques operating in large delay spread channels which span hundreds of symbols and exhibit sparse behavior (i.e., many nearly zero taps) [1], [2]. The combination of multiple-transmit signal processing, i.e., space time/frequency coding, with an orthogonal frequency division multiplexing (OFDM) has been regarded as a promising solution. In particular, OFDM can be archived efficiently by using an inverse fast Fourier transform (IFFT) and FFT. Moreover, it can handle large delay spread channels by transmitting a low-rate data on narrow sub-channels in parallel. On the other hand, the space time/frequency coding can overcome the performance degradation caused by a deep-null effect in such channels. Recently, DVB-T2 system adopted a multiple-input single-output (MISO)-OFDM transmission mode utilizing a space frequency code (SFC) as the standardization [3]–[16]. Despite of its appealing features and applications, the design of a practical OFDM receiver in large delay spread channels is far from being a trivial task. Synchronization, especially symbol timing recovery (STR), represents one of the most challenging issues and plays a major role in the OFDM receiver. In addition, an efficient equalization strategy including a channel frequency estimation is apparently required to provide the desired performance by sufficiently reducing the noise and interference effects.

The OFDM receiver is sensitive to symbol timing offset (STO) effect, which leads to severe inter-symbol interference (ISI) and inter-carrier interference (ICI) problems [6]–[15]. The reliable approaches for resolving these problems are to perform the STR processing with a coarse STR and fine STR, sequentially [6]. The coarse STR is usually performed to initialize the FFT window (or to estimate an initial STO) through a maximum likelihood estimation (MLE) using a guard interval (GI) or a known preamble [7]–[11]. The fine STR is then performed to compensate an inaccurate coarse STO by observing a channel impulse response (CIR) and by analyzing an ambiguity effect of CIR that is caused by an inaccurate coarse STO [13]–[17]. Here, it is noticed that this paper focuses on the fine STR capable of resolving an ambiguity effect in large delay spread channels. Recently, it was shown in [16] that the ambiguity effect can be effectively analyzed and resolved by categorizing possibility that an ambiguity effect occurs, which is predetermined by considering the cases of a false coarse STO under the assumption that the channel maximum delay spread is less than a GI length. Unfortunately, the categorization method does not consider a special channel being longer than the GI, which is specified in [1], [2]. As a result, it will still suffer from the ambiguity effect of CIR in such a channel, which degrades the receiver performance. Thus, an elaborate categorization method is needed to satisfy the requirements of [1], [2].

In performing an equalization, it is noticed that an improved receiver performance can be provided by exploiting the sparse behavior of a channel. In practice, this approach has been researched in a wide variety of time-domain equalizations, named as sparse equalizations, for single-carrier systems. In [20]–[22], it was shown that the sparse equalization can reduce the computational complexities and noise effects by applying various

Manuscript received February 27, 2010; revised October 12, 2010; accepted November 08, 2010. Date of publication December 23, 2010; date of current version February 23, 2011. This work was supported by the IT R&D program of MKE/KEIT. (KI002091, Research on Multiple Antenna and Multi-hop Relay Transmission Technologies for Next Generation Mobile Broadcasting Service), and also by the MKE (The Ministry of Knowledge Economy), Korea, under the ITRC (Information Technology Research Center) support program supervised by the NIPA (National IT Industry Promotion Agency), (NIPA-2010-C1090-1001-0006).

J.-S. Baek is with the Department of Electrical and Computer Engineering, Georgia Institute of Technology, Atlanta, GA 30332 USA (e-mail: jbaek38@ece.gatech.edu; blackgachi@yonsei.ac.kr).

J.-S. Seo is with the Digital Transmission Laboratory, Department of Electrical and Electronic Engineering, Yonsei University, Seoul 120-749, Korea (e-mail: jsseo@yonsei.ac.kr).

Color versions of one or more of the figures in this paper are available online at http://ieeexplore.ieee.org.

Digital Object Identifier 10.1109/TBC.2010.2094310

tap-selection techniques. This approach offers an opportunity for us to apply the basic concept of the sparse equalization for use in a frequency interpolation (FI) filter of an OFDM receiver.

In this paper, we present an improved receiver by proposing a CIR-based fine STR and sparse equalization for a single-input single-output (SISO) and MISO transmission modes of DVB-T2 system. First, the fine STR which considers a special channel condition being larger than the GI is presented based on the CIR estimation and categorization of ambiguity effect of CIR of [16]. For the purpose of minimizing noise and interference effects, a CIR-based sparse equalization is then presented. In the proposed sparse equalization, the sparse behavior of a channel is investigated from the CIR. A basic FI filter implemented with a low-pass filter is shifted or selected according to an echo delay (phase) and maximum delay spread, respectively. As a result, the main principle of the sparse equalization corresponds to the tap-selection techniques of [20]–[22]. Simulation evaluations are accomplished in large delay spread channels causing the ambiguity of CIR and a severe short delay spread channel such as 20-path Rayleigh channel [4]. Furthermore, a single pre-echo channel being longer than the GI, which causes ISI and ICI effects, is specially considered in order to evaluate the robustness of the proposed receiver for SISO transmission mode [1], [2].

II. System Models

We briefly consider a normal MISO carrier mode equipped with a scattered pilot (SP) which includes a normal SISO carrier mode [3]. Let us define the lth symbol of the mth transmitter $\mathrm{G}_m^{\mathrm{tx}}$ as $\{X_{l,k}^m | k = K_{min}, \ldots, (K_{max}-1)\}$, where k denotes a subcarrier index, K_{min} and K_{max} are active subcarrier indices of the first and last active subcarriers, respectively.

A. SP Patterns

In K_{max} subcarriers of $\mathrm{G}_1^{\mathrm{tx}}$, the kth SP, $P_{l,k}^1 = 2A_{sp}(0.5 - r_{l,k})$, where $r_{l,k}$ and A_{sp} denote a reference sequence[1] for generating pilots and the amplitude of the SP, respectively, is defined if the following condition is satisfied [3]

$$k \bmod (D_x D_y) = D_x (l \bmod D_y) \tag{1}$$

where D_x is the separation of pilot bearing carriers and D_y is the number of symbols forming one SP sequence as shown in Fig. 1, where $D_x = 6$ and $D_y = 2$. The SP $P_{l,k}^2$ of $\mathrm{G}_2^{\mathrm{tx}}$ is defined by inverting the phases of $P_{l,k}^1$ as follows

$$P_{l,k}^2 = \begin{cases} P_{l,k}^1, & \text{if } k/D_x \text{ is even} \\ -P_{l,k}^1, & \text{if } k/D_x \text{ is odd.} \end{cases} \tag{2}$$

B. Transmitter and Channel Models

At each transmitter, the symbols are modulated onto IFFT of size N and the GI of length N_g is inserted. The output signal

[1]The reference sequence is derived from a pseudo random binary sequence (PRBS) of which polynomial is $x^{11} + x^2 + 1$. The sequence provides a unique signature in the time-domain for pilot pattern configuration.

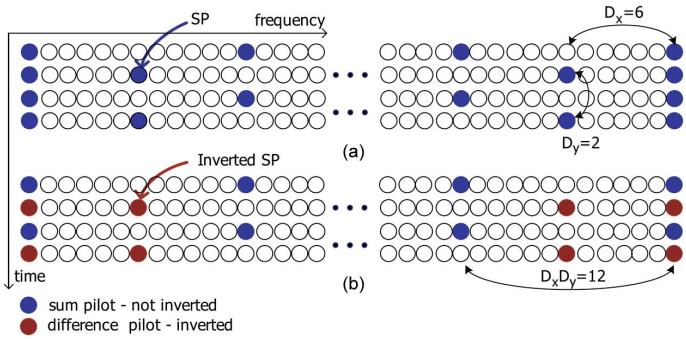

Fig. 1. SP patterns of MISO transmission mode: (a) the SP pattern of $\mathrm{G}_1^{\mathrm{tx}}$; (b) the SP pattern of $\mathrm{G}_2^{\mathrm{tx}}$.

$s^m(t)$ is then transmitted over a multipath channel $h^m(\tau, t)$ modeled as

$$h^m(\tau, t) = \sum_{d=0}^{D^m} h_d^m(t) e^{-j\varphi_d^m} \delta(\tau - \tau_d^m) \tag{3}$$

where $h_d^m(t)$ and φ_d^m denote the dth path complex gain and corresponding phase effect, respectively. τ_d^m is the dth path time delay and D^m is the total number of paths. At a receiver, the sampled signal can be written as

$$r(lT) = \sum_{n=1}^{m} \sum_{d=0}^{D^n} h_d^n(lT) s^n(lT - \tau_d^n) + w(lT) \tag{4}$$

where T is the sampling time interval and $w(lT)$ denotes the sampled white complex Gaussian noise with variance σ_w^2. After removal of the GI, the receiver transforms the remaining N samples into the frequency domain via an FFT. Finally, the kth output subcarrier of the lth OFDM symbol can be represented by

$$Y_{l,k} = \sum_{n=1}^{m} X_{l,k}^n H_{l,k}^n + W_{l,k} \tag{5}$$

where $W_{l,k}$ is the FFT output of $w(lT)$ and $H_{l,k}^n$ is the channel frequency response (CFR).

C. Receiver Model

The proposed receiver structure is depicted in Fig. 2. First, a coarse STR is performed by the MLE in order to estimate an initial STO for the FFT window operation [8]. By performing the time-interpolations (TIs) with a simple linear filter [18], temporal channel frequency responses (CFRs) are estimated for use in the CIRs estimation [16]. The proposed CIR-based fine STR is then performed for the purpose of compensating the coarse STO. In addition, the frequency interpolations (FIs) are performed with a low-pass filter equipped with a sinc filter using the Kaiser window [19]. After an equalization, a signal to noise ratio (SNR) is measured to evaluate the STO effect according to the FFT window [16]. After performing the fine STR, the proposed CIR-based sparse equalization is accomplished through the generation of a FI filter for use in the FIs. In the following sections, the details of the proposed receiver are presented.

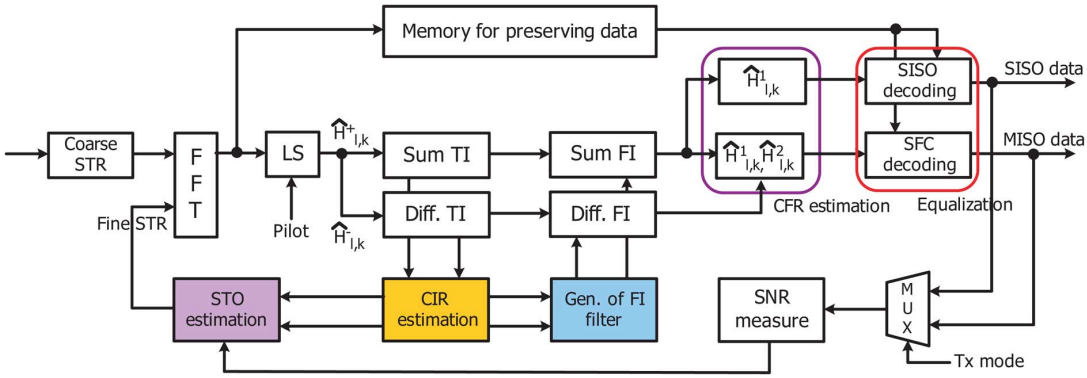

Fig. 2. Proposed receiver structure equipped with the proposed CIR-based fine STR and generation of FI filter for archiving a sparse equalization.

III. CIR Estimations

In this section, we briefly present the CIR estimation that is realized by using the sum TI and difference TI outputs [16]. First, the temporal CFR $\hat{H}^{+}_{l,p}$ and difference CFR $\hat{H}^{-}_{l,p}$ at pilot subcarrier $P^{m}_{l,p} = \{P^{m}_{l,p} | p = 0, \ldots, (N_p - 1)\}$, where N_p is the total number of pilot subcarriers[2], are estimated by using using a least squares (LS) method as follows

$$\begin{aligned} \hat{H}^{+}_{l,p} &\triangleq (\hat{H}^{1}_{l,p} + \hat{H}^{2}_{l,p}) = Y^{+}_{l,p}/P^{1}_{l,p} \\ \hat{H}^{-}_{l,p} &\triangleq (\hat{H}^{1}_{l,p} - \hat{H}^{2}_{l,p}) = Y^{-}_{l,p}/P^{1}_{l,p} \end{aligned} \tag{6}$$

where $Y^{+}_{l,p}$ and $Y^{-}_{l,p}$ are the received sum and difference symbols, respectively. The sum and difference (diff.) TIs are accomplished for $\hat{H}^{+}_{l,p}$ and $\hat{H}^{-}_{l,p}$, respectively as shown in Fig. 2. Then, the CIR is estimated by using the sum and difference TI outputs. Here, the CIR estimation is performed with the non zero-padded IFFT operation of [16] in which the unavailable TI outputs located at the both edges of OFDM symbol are discarded. Let us define the available samples of sum TI output $\{\tilde{H}^{+}_{l,i} | i = 0, \ldots, N_{cir} - 1\}$ and difference TI output $\{\tilde{H}^{-}_{l,i} | i = 0, \ldots, N_{cir} - 1\}$, where IFFT$_{cir}$ size $N_{cir} = 2^n$ is determined if the following condition is satisfied for the SISO and MISO transmission

$$N_{cir} = 2^n, \begin{cases} \text{SISO} & : \text{if } 2^n \le \left(\frac{K_{max}}{D_x} + 1\right) < 2^{n+1} \\ \text{MISO} & : \text{if } 2^n \le \left(\frac{K_{max}}{2D_x} + 1\right) < 2^{n+1}. \end{cases} \tag{7}$$

The sum CIR $\{\hat{h}^{+}_{l,q} | q = 0, 1, \ldots, N_{cir} - 1\}$ is estimated as follows

$$\hat{h}^{+}_{l,q} \triangleq \left(\hat{h}^{1}_{l,q} + \hat{h}^{2}_{l,q}\right) = \sum_{i=0}^{N_{cir}-1} \tilde{H}^{+}_{l,i} e^{j2\pi qi/N_{cir}} \tag{8}$$

where $\{\hat{h}^{1}_{l,q} | q = 0, \ldots, N_{cir} - 1\}$ and $\{\hat{h}^{2}_{l,q} | q = 0, \ldots, N_{cir} - 1\}$ are the estimated CIRs and sampled with a resolution of

$$T' = \left(\frac{N}{D_x N_{cir}}\right) T = \frac{3T}{4} = 0.75T \tag{9}$$

[2]In the notation of $P^{m}_{l,p}$, the index p denotes not the location of an exact pilot subcarrier of (1) but the order of pilot subcarrier in order to explain the principle of CIR estimation of [16].

where the constant 0.75 is applied identically to all transmission modes. The difference CIR $\{\hat{h}^{-}_{l,q} | q = 0, 1, \ldots, N_{cir} - 1\}$ is given by

$$\begin{aligned} \hat{h}^{-}_{l,q} &\triangleq \left(\hat{h}^{1}_{l,q} - \hat{h}^{2}_{l,q}\right) \\ &= \left(\sum_{i=0}^{N_{cir}-1} \tilde{H}^{-}_{l,i} e^{j2\pi qi/N_{cir}}\right) e^{j2\pi qD_x/K_{total}} \end{aligned} \tag{10}$$

where $K_{total} = (K_{min} + K_{max} + 1)$. Here, it is noticed that the difference TI output has a position offset of D_x as compared with the sum TI output. Thus, the effect should be compensated to estimate an accurate CIR, i.e., $\hat{h}^{1}_{l,q}$ and $\hat{h}^{2}_{l,q}$ [16]. Finally, the $\hat{h}^{1}_{l,q}$ and $\hat{h}^{2}_{l,q}$ are estimated from (8) and (10) as follows

$$\begin{aligned} \hat{h}^{1}_{l,q} &= \frac{1}{2}\left(\hat{h}^{+}_{l,q} + \hat{h}^{-}_{l,q}\right) \\ \hat{h}^{2}_{l,q} &= \frac{1}{2}\left(\hat{h}^{+}_{l,q} - \hat{h}^{-}_{l,q}\right). \end{aligned} \tag{11}$$

IV. Proposed CIR-Based Fine STR

A. Method for Resolving Ambiguity Effect of CIR

We present a method for resolving the ambiguity effect of CIR (exactly total sum CIR). It was shown in [16] that the ambiguity effect can be effectively analyzed and resolved by categorizing possibility that an ambiguity effect occurs, which is predetermined by considering the cases of a false coarse STO. From this point of view, we categorize the ambiguity effect of CIR. Here, the categorization of ambiguity effect is presented based on the sum power of CIR given by

$$\left|\hat{h}_{l,q}\right|^2 = \left|\hat{h}^{1}_{l,q}\right|^2 + \left|\hat{h}^{2}_{l,q}\right|^2. \tag{12}$$

Fig. 3 illustrates five cases by assuming that each channel corresponding to $h^{m}_{l,q}$ has a single-echo [4]. In particular, Fig. 3(a) illustrates Cases $\mathtt{I}_s$, $\mathtt{II}_s$, and $\mathtt{III}_s$ by assuming that the maximum delay spread of channel is within the GI. These cases are applied identically to the SISO and MISO transmission modes. On the other hand, Cases $\mathtt{IV}_s$ and $\mathtt{V}_s$ shown in Fig. 3(b) are illustrations of the SISO transmission mode by considering a

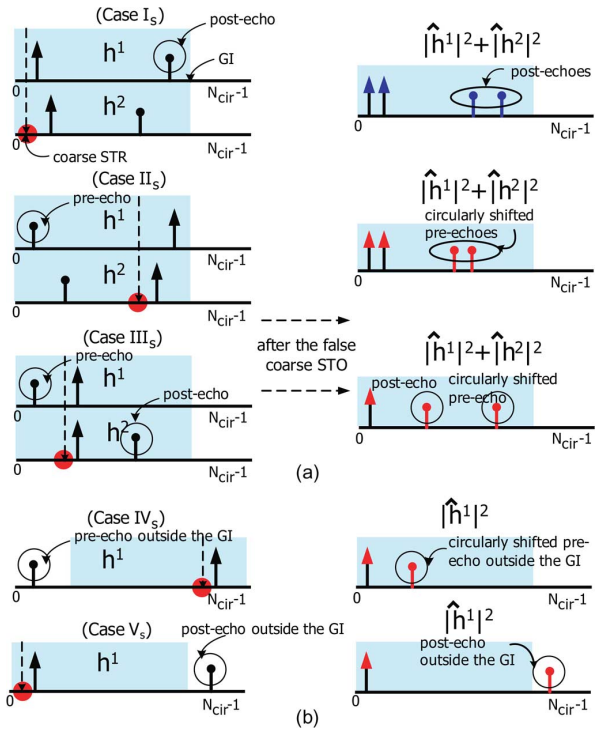

Fig. 3. Ambiguity effect of CIR: (a) ambiguity effect under assumption that channel is within the GI; (b) ambiguity effect under assumption that channel is outside the GI.

pre/post single-echo outside the GI of which channel condition is strictly required in [1], [2].

- Case $\mathtt{I}_s$ (**post-echo case**)Case $\mathtt{I}_s$ is considered by assuming that a channel consists of post-echoes without a pre-echo. It is also assumed that the power of post-echoes is smaller than that of main-path. In this case, the coarse STR may not cause the ambiguity effect of $|\hat{h}_{l,q}|^2$ even though a STO occurs in the ISI-free FFT window region [14]. Thus, the fine STO can be achieved with a single change of the FFT window.
- Case $\mathtt{II}_s$ (**pre-echo case**)Case $\mathtt{II}_s$ assumes that a channel has one more weak pre-echoes as compared with main-path. In this assumption, the coarse STR may determine the FFT window around the main-path, which induces the circularly shift of the observation window [16]. As a result, the ambiguity is in the circularly shifted pre-echoes as shown in the second figure of Fig. 3(a). Moreover, the pre-echoes could be regarded as post-echoes as in Case $\mathtt{I}_s$. Accordingly, at least two changes of the FFT window are required in order to verify whether the echoes are circularly shifted pre-echoes or post-echoes.
- Case $\mathtt{III}_s$ (**pair-echo case**)Case $\mathtt{III}_s$ considers a weak pair-echo channel where the distance between pre-echo and main-path is nearly equal to the distance between main-path and post-echo [1]. This channel corresponds to the combination of Cases $\mathtt{I}_s$ and $\mathtt{II}_s$. In the third figure of Fig. 3(a), it is found that the ambiguity is in the circularly shifted pre-echo. In addition, the post-echo could be regarded as the circularly shifted pre-echo as in Case $\mathtt{II}_s$ when the post-echo path delay in a reduced scale is longer than $N_{cir} - \lceil (3/4)N_g \rceil - 1$ [ref. (13)]. Moreover, the echoes could be regarded as post-echoes. Thus, at least two changes of the FFT window are required in order to resolve the ambiguity of CIR.
- Case $\mathtt{IV}_s$ (**pre-echo outside the GI case**)Case $\mathtt{IV}_s$ considers a weak single pre-echo outside the GI [1]. Here, it is expected that the coarse STO may induce the circularly shift of the pre-echo outside the GI as shown in the first figure of Fig. 3(b). This configuration can be regarded as in Case $\mathtt{I}_s$ Thus, the verification procedure of Case $\mathtt{II}_s$ is also required.
- Case $\mathtt{V}_s$ (**post-echo outside the GI case**)Case $\mathtt{V}_s$ is the other special channel having a weak post-echo outside the GI [1]. In this case, the coarse STO may not cause the ambiguity effect. However, the post-echo outside the GI could be regarded as a circularly shifted pre-echo, which requires a similar verification procedure with Case $\mathtt{IV}_s$.

From the above cases, we categorize the ambiguity effect of $|\hat{h}_{l,q}|^2$ by investigating the overlapped and non-overlapped regions, where the region of each case is determined by the maximum channel delay satisfying the corresponding assumptions. Fig. 4 categorizes the ambiguity effect into six regions $\{R_a, R_b, R_c, R_d, R_e, R_f\}$ where the boundary values $D = \{D_a, D_b, D_c, D_d, D_e, D_f\}$ of each region[3] are defined as

$$D = \begin{cases} D_a = N_{cir} - \lceil 0.75\rho(T_u/D_x T) \rceil - 1 \\ D_b = N_{cir} - \lceil 0.75 N_g \rceil - 1 \\ D_c = N_{cir} - \lceil (0.75/2) N_g \rceil - 1 \\ D_d = \lceil 0.75 N_g \rceil - 1 \\ D_e = \lceil 0.75\rho(T_u/D_x T) \rceil - 1 \\ D_f = N_{cir} - 1 \end{cases} \quad (13)$$

where T_u is the total symbol duration and ρ is the pass-band to stop-band ratio of a filter for use in FIs. $\lceil x \rceil$ is the closest integer value that is greater than or equal to the value of x. Accordingly, if an echo is detected in regions R_a or R_f, single change of the starting position of FFT window is accomplished. If an echo is detected in the other regions, two changes are accomplished by investigating whether it is a post-echo or a circularly shifted pre-echo/pre-echo outside the GI. On the other hand, it is noticed that the change operation is very inefficient if many echoes exist in a region. Moreover, if the echo delay is not an exact integer time of T, which means that an echo power will be dispersed, it is difficult to detect a weak echo correctly [1]. For the purpose of minimizing these problems, echo detection methods are proposed herein. First, a differential detection is performed with one sample delay in order to sum the dispersed powers of $|\hat{h}_{l,q}|^2$ as follows

$$\left|\hat{h}'_{l,q}\right|^2 = \left|\hat{h}_{l,q}\right|^2 + \left|\hat{h}_{l,q+1}\right|^2, \quad \text{if} \quad \left|\hat{h}'_{l,q}\right|^2 \geq \left|\hat{h}_{l,q}\right|^2. \quad (14)$$

A simple threshold method is then applied to $|\hat{h}'_{l,q}|^2$ as follows

$$\left|\hat{h}'_{l,q}\right|^2 = \begin{cases} \left|\hat{h}'_{l,q}\right|^2, & \text{if } \left|\hat{h}'_{l,q}\right|^2 \geq \delta_{th} \\ 0, & \text{otherwise} \end{cases} \quad (15)$$

[3]In each case of Fig. 4, the boundary is determined by a maximum distance (the number of sample) of causable echo when a false STO occurs. More simple case is presented in [16].

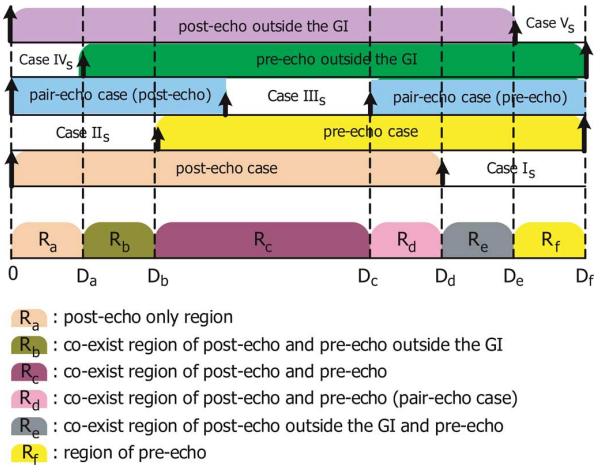

Fig. 4. Categorization of ambiguity effect of CIR.

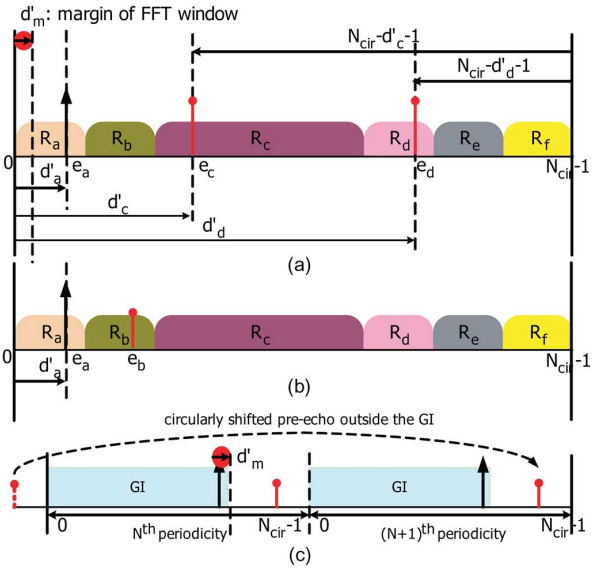

Fig. 5. Illustration of the fine STO estimation: (a) fine STO estimation for the case of echoes within the GI; (b) fine STO estimation for the case of pre-echo outside the GI; (c) required fine STO estimation.

where δ_{th} denotes the threshold value. Finally, an echo e_r which is the nearest echo with zero out of detected echoes in the region is detected as follows

$$e_r \leftarrow d'_r = min(d'_{r,s}), \quad \text{for} \quad r = a, b, c, d, e, f \text{ and } s = 1, 2 \ldots \tag{16}$$

where $d'_{r,s}$ represents the distance between the zero-point marked in Figs. 4 and 5 and the sth echo in the rth region, $e_{r,s}$. $min(\cdot)$ denotes the minimum operation. This method does not cause the ISI problem even though STO occurs in the ISI-free FFT window region.

B. Illustration of the Fine STO Estimation for the Case of Echoes Within the GI

For the comprehensive understanding, we illustrate the overall operation process of the proposed fine STR for estimating the fine STO in a channel causing the ambiguity effect. Let us assume that $|\hat{h}_{l,q}|^2$ is given by Fig. 5(a) after applying the coarse STR, (15), and (16). This CIR configuration relates to `Case` $\mathtt{III}_s$. Thus, in order to resolve the ambiguity effect observed in echoes e_c and e_d, three changes of the FFT window are needed. First, the FFT window is successively changed twice by regarding the echoes e_c and e_d as the circularly shifted pre-echoes. Here, each STO $\triangle\hat{\theta}_r^{pre}$ is calculated in an enlarged scale as follows

$$\Delta\hat{\theta}_r^{pre} = -\left\lceil \frac{4}{3}\left(d'_m + N_{cir} + d'_r + 1\right)\right\rceil \quad \text{for } r = c, d \tag{17}$$

where d'_m represents the margin of FFT window. After applying each $\triangle\hat{\theta}_r^{pre}$, SNR $\gamma(\triangle\hat{\theta}_r^{pre})$[4] in Fig. 2 is measured to estimate the fine STO providing a maximum SNR. Then, by regarding those as post-echoes, the change of the starting position of FFT window is performed with $\triangle\hat{\theta}_a^{post}$ calculated as

$$\Delta\hat{\theta}_a^{post} = \left\lceil \frac{4}{3}\left(d'_m - d'_a\right)\right\rceil. \tag{18}$$

In addition, $\gamma(\triangle\hat{\theta}_a^{post})$ is also measured. Finally, after performing the above processes, we compare the measured SNRs as follows

$$\Delta\hat{\theta} \leftarrow \gamma(\Delta\hat{\theta}) = max\left(\gamma\left(\Delta\hat{\theta}_c^{pre}\right), \gamma\left(\Delta\hat{\theta}_d^{post}\right), \gamma\left(\Delta\hat{\theta}_a^{post}\right)\right) \tag{19}$$

where $max(\cdot)$ denotes the maximum operation. If $\gamma(\triangle\hat{\theta}_r^{pre})$ has a maximum SNR, the FFT window is changed once again with $\triangle\hat{\theta}_r^{pre}$. Whereas, if $\gamma(\triangle\hat{\theta}^{post})$ has a maximum SNR, FFT window is preserved. Though, we illustrate a special case, the aforementioned fine STR processes can be identically applied to any ambiguity effects.

C. Illustration of the Fine STO Estimation for the Case of Pre-Echo Outside the GI

Let us illustrate a special `Case` $\mathtt{IV}_s$ as depicted in Fig. 5(b). It is shown that the ambiguity effect appears in the circularly shifted pre-echo outside the GI e_b. Therefore, the FFT window has to be changed twice with e_b and e_a. Here, it is noticed that though the ISI and ICI effects in this channel are inevitable, these effects could be minimized by adjusting properly the FFT window as shown in Fig. 5(c). That is, FFT window has to be determined so as to capture an echo having relatively higher power than the other in FFT window and minimize the amount of ISI caused by adjacent OFDM symbols [11]. In order to satisfy these requirements, $\triangle\hat{\theta}_b^{pre'}$ is calculated as follows

$$\Delta\hat{\theta}_b^{pre'} = -\left\lceil \frac{4}{3}(N_g - d_a - d_m - 1)\right\rceil. \tag{20}$$

On the other hand, $\triangle\hat{\theta}_a^{post}$ is calculated identically with (18). After measuring $\gamma(\triangle\hat{\theta}_b^{post'})$ and $\gamma(\triangle\hat{\theta}_a^{post})$, the fine STO providing a maximum SNR is estimated as follows

$$\Delta\hat{\theta} \leftarrow \gamma(\Delta\hat{\theta}) = max\left(\gamma\left(\Delta\hat{\theta}_b^{pre'}\right), \gamma\left(\Delta\hat{\theta}_a^{post}\right)\right). \tag{21}$$

The following processes are identical with Fig. 5(a).

[4]In the followings, $\gamma(\triangle\hat{\theta})$ denotes the measured SNR after changing the FFT window with $\triangle\hat{\theta}$.

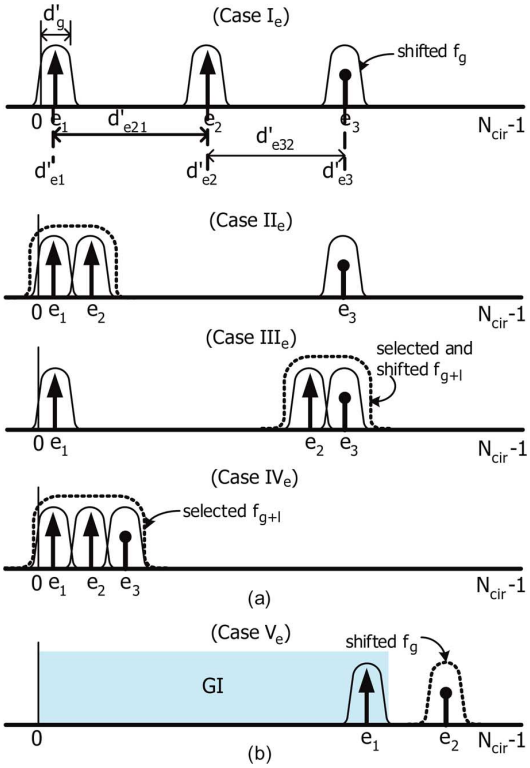

Fig. 6. Cases of CIR-based generation of FI filter for archiving the proposed sparse equalization.

V. Proposed CIR-Based Sparse Equalization

In this section, we present the CIR-based generation method of FIs filter for use in the sum and difference FIs [ref. Fig. 2], which ultimately archives the proposed sparse equalization upon completing the fine STR. Here, it is noticed that the useful CIRs in MISO transmission mode are $|\hat{h}^{+'}_{l,q}|^2$ and $|\hat{h}^{-'}_{l,q}|^2$ after applying (14) and (15) to (8) and (10), respectively. The main advantage of the proposed CIR-based FI is to use conventional FI filters implemented with various GI fractions $gi \in \{1/128, 1/32, 1/16, 19/128, 1/8, 19/128, 1/4\}$ [3]. Let us define the FI filter $\{f_{g,k}|k = -0.5N_f, \ldots, 0.5N_f\}$ where N_f is the length of a low-pass filter and the index $g \in \{1,2,3,4,5,6,7\}$ denotes each GI fraction of gi in order. The valid bandwidth of FI filter in the time-domain, d'_g marked in Fig. 6, is defined at a reduced scale as follows

$$d'_g = \left\lceil 0.75\rho \frac{N_g T g i}{2} \right\rceil \triangleq \left\lceil 0.75\rho \frac{B_t}{2} \right\rceil \tag{22}$$

where $B_t = N_g T(gi)$. Fig. 6 illustrates the five cases of the generation of FI filter according to the sparse behavior and maximum delay spread of the CIR power. The Cases $\mathtt{I}_e$, $\mathtt{II}_e$, $\mathtt{III}_e$, and $\mathtt{IV}_e$ of Fig. 6(a) can be applied to Cases $\mathtt{I}_s$, $\mathtt{II}_s$, $\mathtt{III}_s$, and $\mathtt{IV}_s$ of Fig. 3. On the other hand, Case $\mathtt{V}_e$ of Fig. 6(b) is specially applied to Case $\mathtt{IV}_s$.

A. Generation of FI Filter

For the comprehensive understanding of the basic principle of the generation of FI filter, $\{F_{s,k}|k = -0.5N_f, \ldots, 0.5N_f\}$, we assume that three paths are found in Cases $\mathtt{I}_e$, $\mathtt{II}_e$, $\mathtt{III}_e$, and $\mathtt{IV}_e$. In Fig. 6, each case illustrates the generation method of FI filter by shifting or selecting a basic filter f_g according to an echo delay d'_{e_i} and a distance between echoes $d'_{e_{ji}}$ defined as

$$d'_{e_{ji}} = \left| d'_{e_j} - d'_{e_i} \right| \triangleq \left| d'_{e_{i+1}} - d'_{e_i} \right| \quad \text{for} \quad i = 1,2,3. \tag{23}$$

First, f_g having a small d'_g such as $g = 1,2$ is predetermined in order to reduce the noise effects as much as possible. After estimating d'_{e_i} and $d'_{e_{ji}}$, the condition between $d'_{e_{ji}}$ and d'_g is investigated whether each echo is separated sufficiently so as to avoid the overlap of f_g and to shift f_g. If a condition is satisfied, f_g is shifted as much as the echo delay. However, if it does not be satisfied, the other basic filter $f^s_g = f_{g+l}$ $(l \geq 1)$ having a bigger d'_{g+l} is selected and the same checking procedure is accomplished. Finally, the selected or shifted basic filters are summed to generate FI filter. In the following, the aforementioned procedures are categorized for each case.

- Case $\mathtt{I}_e$: if $(d'_{e_{21}} \geq d'_g) \bigcap (d'_{e_{32}} \geq d'_g)$

$$F_{s,k} = \sum_{i=1}^{3} f_{g,k} e^{-j2\pi k d_{e_i}/N} \tag{24}$$

  where $d_{e_i} = \lceil (4/3) d'_{e_i} \rceil$.
- Case $\mathtt{II}_e$: if $(d'_{e_{21}} < d'_g) \bigcap (d'_{e_{32}} \geq d'_g)$

$$F_{s,k} = f^s_{g,k} e^{-j\pi k(d_{e_1}+d_{e_2})/N} + f_{g,k} e^{-j2\pi k d_{e_3}/N} \tag{25}$$

  where f^s_g is the basic filter satisfying $(d'_g < d'_{e_{21}} \leq d'_{g+1})$.
- Case $\mathtt{III}_e$: if $(d'_{e_{21}} \geq d'_g) \bigcap (d'_{e_{32}} < d'_g)$

$$F_{s,k} = f_{g,k} e^{-j2\pi k d_{e_1}/N} + f^s_{g,k} e^{-j\pi k(d_{e_2}+d_{e_3})/N} \tag{26}$$

  where f^s_g is the basic filter satisfying $(d'_g < d'_{e_{32}} \leq d'_{g+1})$.
- Case $\mathtt{IV}_e$: if $(d'_{e_{21}} < d'_g) \bigcap (d'_{e_{32}} < d'_g)$

$$F_{s,k} = f^s_{g,k} e^{-j\pi k(d_{e_1}+d_{e_3})/N} \tag{27}$$

  where f^s_g is the basic filter satisfying $(d'_g < d'_{e_{31}} \leq d'_{g+1})$.Next, we consider Case $\mathtt{V}_e$, where it is assumed that the single pre-echo outside the GI is found. This case performs a similar procedure as the above cases except that the shift direction of f_g is opposite. Moreover, the purpose of the generation of FI filter is to further alleviate the ISI and ICI effects.
- Case $\mathtt{V}_e$: if $(d'_{e_{21}} \geq d'_g)$

$$F_{s,k} = f_{g,k} e^{-j\pi k d_{e_1}/N} + f_{g,k} e^{j\pi k \bar{d}_{e_2}/N} \tag{28}$$

  where $\bar{d}_{e_i} = \lceil (4/3)(N_{cir} - d'_{e_i}) \rceil$.

Here, it is noticed that even though we assume three paths, the basic principle could be expanded to more complex echoes at the expense of additional logics for investigating much more conditions. However, the portion of the logics is very small in the total hardware complexity. Thus, we assert that the proposed sparse equalization is very efficient.

VI. Performance Evaluations

The choice of parameters of SISO and MISO transmission modes of DVB-T2 system is dictated by the network deployment such as the GI duration, bandwidth, and pilot pattern mode.

TABLE I
SIMULATION CONDITIONS

Transmission mode G_m^t	SISO, MISO
Carrier mode	normal mode
Bandwidth	8MHz ($T = 7/64\mu s$)
FFT size N	32K (32,768)
Symbol duration T_u	32K·T
No. of subcarriers	$K_{min} = 0$, $K_{max} = 27,264$
GI fraction gi	1/128 (PP7), 19/256 (PP2)
Modulation	4-QAM, 16-QAM, 64-QAM, 256-QAM
Pilot pattern (PP) mode	PP2 ($D_x = 6, D_y = 2$), $A_{sp} = 4/3$
	PP7 ($D_x = 24, D_y = 4$), $A_{sp} = 7/3$
Length of FI filter N_f	480 (1/128-gi)
CIR size N_{cir}	4096 (PP2), 1024 (PP7)
Channel model	3-path echo ($19/256$-gi)
	20-path Rayleigh [4]
	pre-echo outside the GI ($1/128$-gi) [1]

TABLE II
CHANNEL MODELS CAUSING THE AMBIGUITY EFFECT OF CIR

channels (SISO)	parameters	path-1	path-2	path-3
C-I (Case $\mathtt{II}_s$)	$\tau^1[\mu s]$	-253	-126	0
	h^1 [dB]	-3	-6	0
	$\varphi^1[^\circ]$	90	0	0
C-II (Case $\mathtt{III}_s$)	$\tau^1[\mu s]$	-127	0	126
	h^1 [dB]	-3	0	-6
	$\varphi^1[^\circ]$	90	0	0
C-III (Case $\mathtt{IV}_s$)	$\tau^1[\mu s]$	$-\tau_1^1$	0	·
	h^1 [dB]	$-h_1^1$	0	·
	$\varphi^1[^\circ]$	90	0	·
channels (MISO)	**parameters**	**path-1**	**path-2**	**path-3**
C-IV (Case $\mathtt{II}_s$)	$\tau^1[\mu s]$	-127	0	·
	h^1 [dB]	-3	0	·
	$\varphi^1[^\circ]$	0	0	·
(Case $\mathtt{I}_s$)	$\tau^2[\mu s]$	0	126	·
	h^2 [dB]	0	-6	·
	$\varphi^2[^\circ]$	0	90	·

Computer simulations were conducted to verify the effectiveness and robustness of the proposed receiver under the simulation conditions listed in Table I. Parameters of the OFDM transmission basically follow the DVB-T2 standard, and the modulation schemes 4-QAM, 16-QAM, 64-QAM and 256-QAM were adopted to evaluate the variation trends of symbol error rate (SER) performance according to the various bit-rates. The length of sinc filter using the Kaiser window for use in the FIs, $N_f = 480$, was chosen from simulations in white Gaussian noise channel with a Kaiser factor $K_w = 5$ providing a sufficient SNR higher than 40 dB. Here, the filter of 3 dB bandwidth was set to $0.5 \cdot 0.87B_t$ [ref. (22)], where $\rho = 0.87$. In order to demonstrate the overall operation process of the proposed fine STR illustrated in Fig. 5, we modeled the large delay spread channels listed in Table II. Channels C-I and C-II for use in the SISO transmission mode corresponds to Cases $\mathtt{II}_s$ and $\mathtt{III}_s$, respectively. Channel IV is for use in the MISO transmission mode, where h^1 and h^2 belong to Cases $\mathtt{II}_s$ and $\mathtt{I}_s$, respectively. For these channels, it was assumed that a maximum delay spread is 95 percentage of N_g [1]. In addition, we modeled channel C-III which corresponds to Case $\mathtt{IV}_s$, and the path gain and time delay were varied in order to evaluate the robustness of the proposed receiver according to the parameters. Finally, we adopted the 20-path Rayleigh channels defined in DVB-T2 specification [4] for both the transmission modes in order to evaluate the SER performance of a receiver in short delay spread channel. This channel is generally used to describe the portable indoor or outdoor reception conditions. It does not include any Doppler and should therefore be considered as a snapshot of the real-time Rayleigh channel.

A. SISO Transmission Mode: Pre-Echo Within the GI

Performance evaluations of the proposed fine STR and sparse equalization are accomplished for SISO transmission mode. We choose parameters 19/256-gi, 256-QAM, and PP2 mode. In addition, $d_m = 15$, $\delta_{th} = 0.0032$, and $N_{cir} = 4\,\mathrm{K}$ are assumed to estimate the CIR [ref. (7)].

We first evaluate the performance of the proposed fine STR. Fig. 7 depicts the operation process of the proposed fine STR for archiving the fine STO in channel C-I with an input SNR of 30 dB. Fig. 7(c) shows that the pre-echoes look as if those are post-echoes after the coarse STR. It is shown that the ambiguity effect is in the circularly shifted pre-echoes. Therefore, in order to resolve the effect, the region including each echo is first checked by using (13). Then, the FFT window is changed successively with the STO estimated by (17) and (18). Fig. 7(a) depicts the change process of the FFT window in terms of the change process of the CIR $|\hat{h}^{1'}|^2$ [ref. (15)] in order $\triangle\hat{\theta}_c^{pre} \rightarrow \triangle\hat{\theta}_d^{pre} \rightarrow \triangle\hat{\theta}_a^{post}$. In addition, the change process of $\gamma(\triangle\hat{\theta})$, i.e., $\gamma(\triangle\hat{\theta}_c^{pre}) \rightarrow \gamma(\triangle\hat{\theta}_d^{pre}) \rightarrow \gamma(\triangle\hat{\theta}_a^{post})$, is also depicted. Finally, after performing three change processes, the measured SNRs are compared to estimate the fine STO. Here, it is noticed that $(2D_y - 1)$ symbols are taken to obtain the exact SNR according to the use of each STO by discarding the past symbols and fulfilling the new symbols into the TI after changing the FFT window. In Fig. 7(b), it is observed that $\triangle\hat{\theta}_c^{pre}$ provides the maximum SNR, thus the FFT window is once more changed with $\triangle\hat{\theta}_c^{pre}$ to achieve the fine STO. Fig. 7(c) shows $|\hat{h}^{1'}|^2$ after fine STR, which proves that the proposed fine STR resolved the ambiguity effect.

We evaluate the performance of the proposed fine STR in channel C-II, where simulation conditions are identical with Fig. 7. Fig. 8(c) shows that the CIR configuration is similar with Fig. 7(c), and the ambiguity effect is in the circularly shifted pre-echo. Thus, the fine STR takes a similar change process of FFT window in order $\triangle\hat{\theta}_c^{pre} \rightarrow \triangle\hat{\theta}_d^{pre} \rightarrow \triangle\hat{\theta}_a^{post}$, and correspondingly $\gamma(\triangle\hat{\theta}_c^{pre}) \rightarrow \gamma(\triangle\hat{\theta}_d^{pre}) \rightarrow \gamma(\triangle\hat{\theta}_a^{post})$. On the other hand, it is found in Fig. 8(b) that $\triangle\hat{\theta}_d^{pre}$ provides the maximum SNR, thus the FFT window is further changed with $\triangle\hat{\theta}_d^{pre}$ to achieve the fine STO.

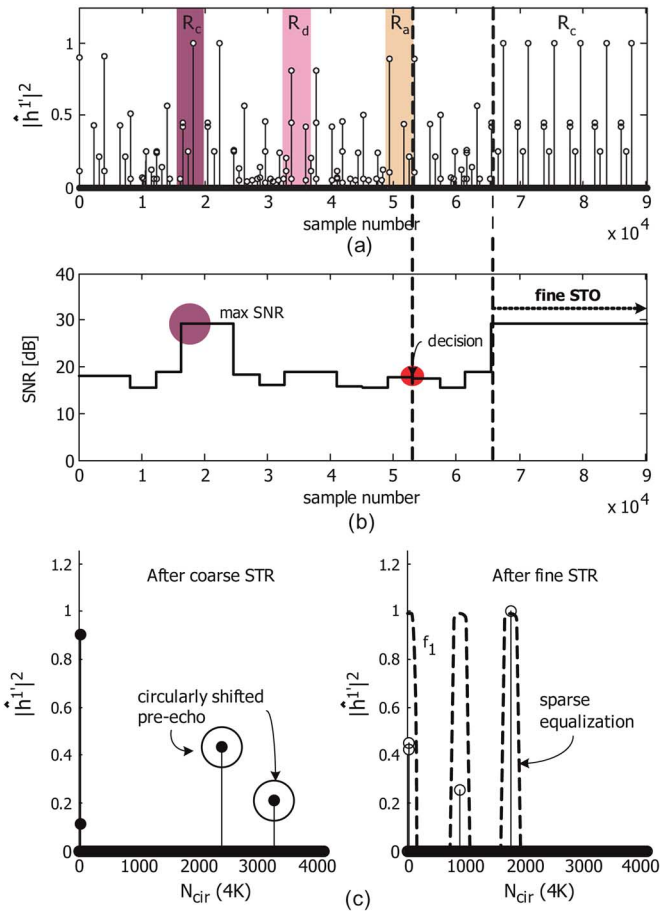

Fig. 7. Proposed fine STR for achieving the fine STO in channel C-I in SISO transmission mode. (a) The change process of $|\hat{h}^{1'}|^2$. (b) The change process of $\gamma(\triangle\hat{\theta})$. (c) $|\hat{h}^{1'}|^2$ before and after the fine STR.

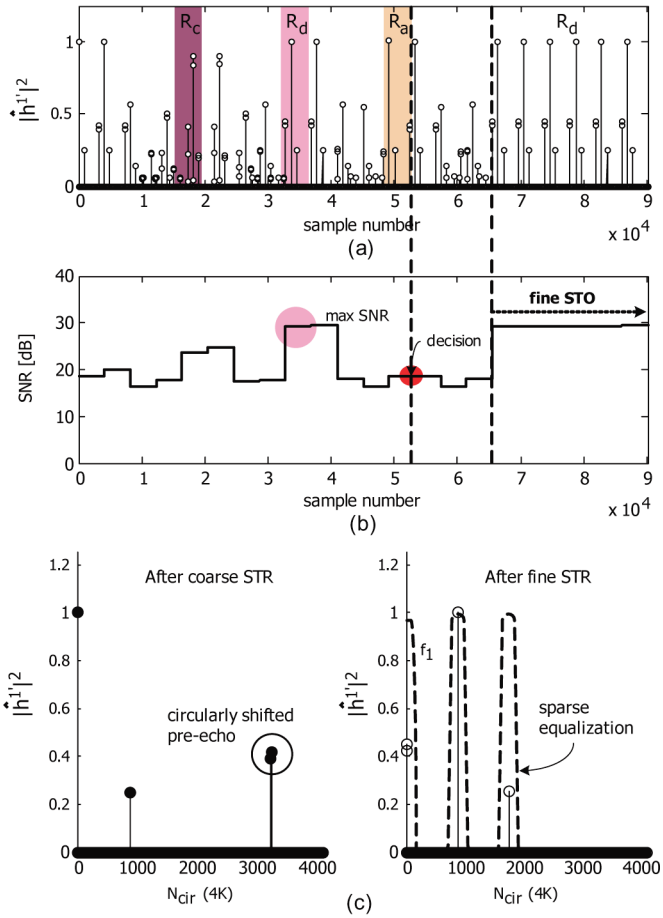

Fig. 8. The proposed fine STR for achieving the fine STO in channel C-II in SISO transmission mode. (a) The change process of $|\hat{h}^{1'}|^2$. (b) The change process of $\gamma(\triangle\hat{\theta})$. (c) $|\hat{h}^{1'}|^2$ before and after the fine STR.

Next, we show the SER performance of the proposed sparse equalization in the channel C-I. For the generation of FI filter, the basic FI filter is firstly set to $f_g = f_1$ (1/128-gi). Then, the sparse behavior of the channel C-I is invested from the CIR after fine STR of Fig. 7(c). It is found that the channel C-I corresponds to Case I_e of Fig. 6, and thus the FI filter is generated by (24). Fig. 9 depicts the SER curves of the sparse equalization and conventional equalization that uses FI filter corresponding to 19/256-gi as the function of the input SNR for 4-QAM, 16-QAM, 64-QAM and 256-QAM modulation schemes. In addition, the optimum SER performance is provided by assuming that a channel information is perfectly known to the receiver. From Fig. 9, we can see that the proposed sparse equalization improves the SER performance by reducing the noise as compared to the conventional equalization. Moreover, the performance is close to optimum performance. The proposed sparse equalization in the channel C-II shows a similar SER performance.

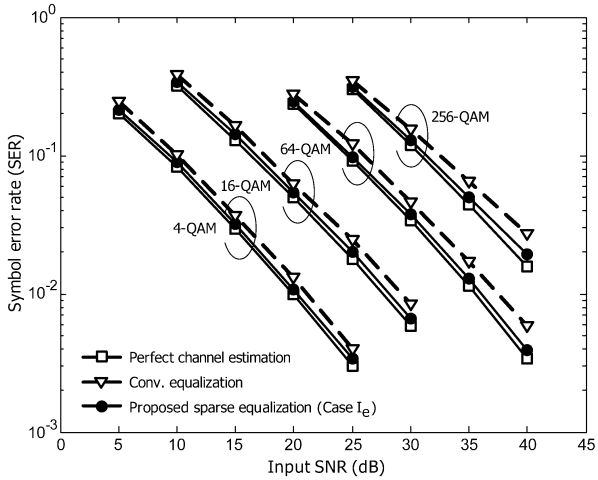

Fig. 9. SER curves of various equalizations as the function of the input SNR for 4-QAM, 16-QAM, 64-QAM, and 256-QAM.

B. MISO Transmission Mode: Pre-Echo Within the GI

The performance evaluations of the MISO transmission mode are conducted. Simulation conditions of the proposed fine STR and sparse equalization are identical with Fig. 7 except $N_{cir} = 2\,\mathrm{K}$ from (7).

Fig. 10 shows the operation process of the proposed fine STR in channel C-IV. Here, it is expected from Fig. 7 that after the coarse STR, the ambiguity effect is in the circularly shifted pre-echo of h^1. Moreover, the CIR configuration is similar with Figs. 7(c) and 8(c). That is, the echoes are observed in regions $R = \{R_c, R_d, R_a\}$. The fine STR changes FFT window in

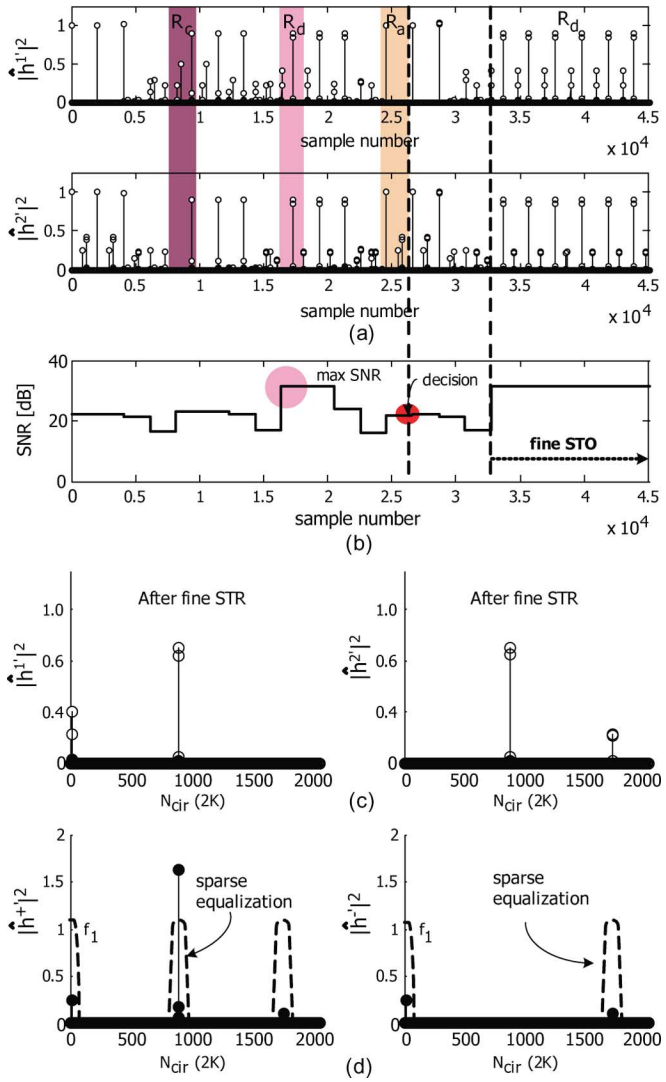

Fig. 10. Proposed fine STR for achieving the fine STO for channel C-IV in MISO transmission mode. (a) The change processes of $|\hat{h}^{1'}|^2$ and $|\hat{h}^{2'}|^2$. (b) The change process of $\gamma(\triangle\hat{\theta})$. (c) $|\hat{h}^{1'}|^2$ and $|\hat{h}^{2'}|^2$ after the fine STR (d) $|\hat{h}^{+'}|^2$ and $|\hat{h}^{-'}|^2$ after the fine STR.

order $\triangle\hat{\theta}_c^{pre} \rightarrow \triangle\hat{\theta}_d^{pre} \rightarrow \triangle\hat{\theta}_a^{post}$, and correspondingly $\gamma(\triangle\hat{\theta}_c^{pre}) \rightarrow \gamma(\triangle\hat{\theta}_d^{pre}) \rightarrow \gamma(\triangle\hat{\theta}_a^{post})$. After comparing the measured SNRs, the FFT window is further changed with $\triangle\hat{\theta}_d^{pre}$ to achieve the fine STO as shown in Fig. 10(a). The fine STO can be verified from Fig. 10(c).

The SER performance of the proposed sparse equalization is shown to compare with that of the conventional equalization. It is noticed that the sparse behavior of the channel C-IV for use in the sum and difference FIs is investigated from $|\hat{h}^{+'}|^2$ and $|\hat{h}^{-'}|^2$, respectively, as shown in Fig. 10(d). We can see that the sparse behaviors of $|\hat{h}^{+'}|^2$ and $|\hat{h}^{-'}|^2$ correspond to `Case` $\mathtt{I}_e$ of Fig. 6. Thus, the FI filters for the sum and difference FIs are generated by (24). From Fig. 11, we can see that the proposed sparse equalization improves the SER performance by $1 \sim 2$ dB as compared with the conventional equalization.

Furthermore, we show the SER performance comparison in 20-path MISO Rayleigh channel, where the maximum delay spread is within about 5 μs. For the purpose of analyzing the

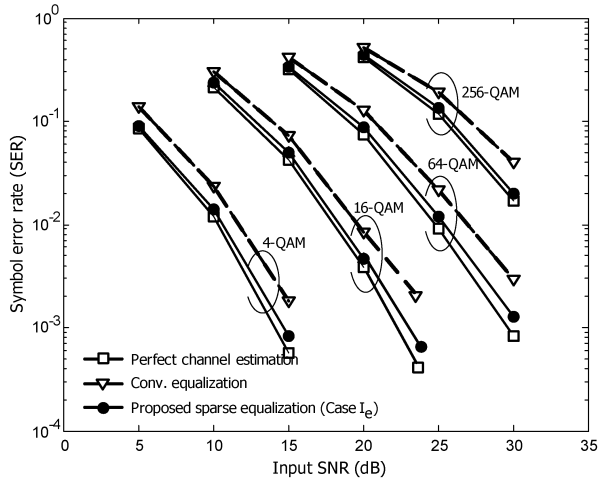

Fig. 11. SER curves of various equalizations as the function of the input SNR for 4-QAM, 16-QAM, 64-QAM, and 256-QAM.

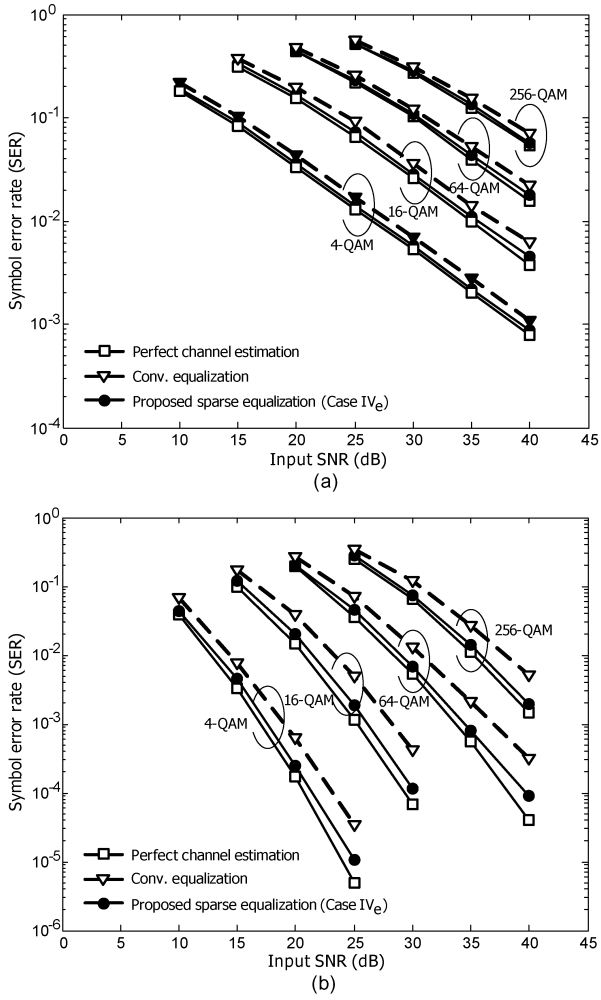

Fig. 12. SER curves of various equalizations as the function of the input SNR for 4-QAM, 16-QAM, 64-QAM, and 256-QAM (a) SISO transmission mode. (b) MISO transmission mode.

performance of the proposed sparse equalization with multiple transmit antenna, comparison in 20-path SISO Rayleigh channel is considered as well [4]. In these channels, it is noticed

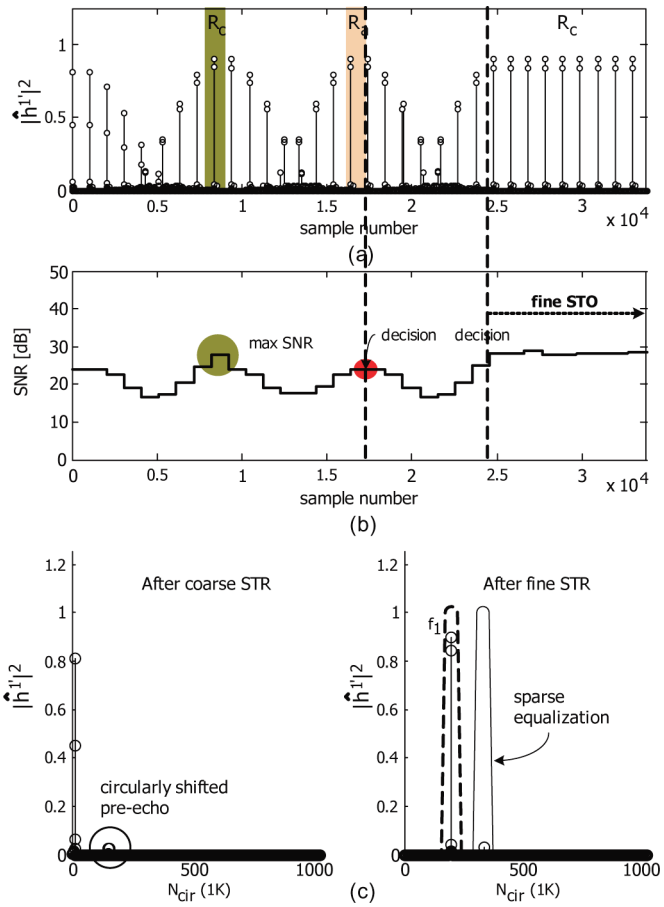

Fig. 13. Proposed fine STR for achieving the fine STO in channel C-III in SISO transmission mode. (a) The change process of $|\hat{h}^{1'}|^2$. (b) The change process of $\gamma(\triangle\hat{\theta})$. (c) $|\hat{h}^{1'}|^2$ before and after the fine STR.

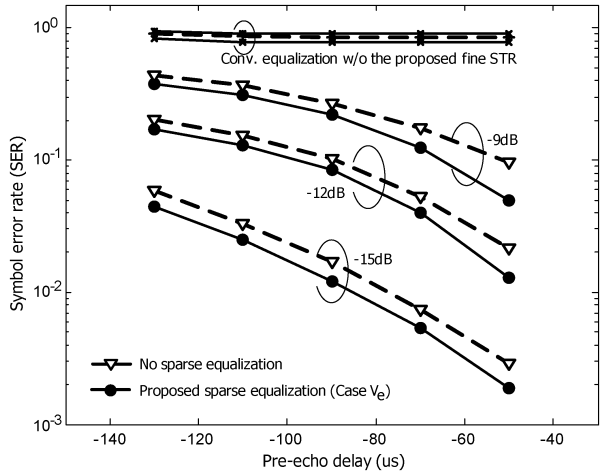

Fig. 14. SER curves of various equalizations as the function of the pre-echo delay (τ_1^1) when h_1^1 is $-9/-12/-15$ dB.

that shifting f_1 causes the overlap of filters, which leads to performance degradation due to the clustered echoes within 5 μs. Thus, FI filter generated by (27) of Case $\mathtt{VI}_s$ is applied. Fig. 12 illustrates that the proposed sparse equalization outperforms the conventional equalization in MISO transmission mode. This performance gain is attributed by the fact that the noise effects are further reduced by using sum and difference FI filters.

C. SISO Transmission Mode: Pre-Echo Outside the GI

Finally, we evaluate the performance of the proposed fine STR and sparse equalization in the channel III. Simulation parameters were 1/128-gi, 256-QAM, PP7 mode [1], $d_m = 15$, $\delta_{th} = 0.003$, $N_{cir} = 1$ K, and $f_b = f_1$. It was assumed that $\tau_1^1 \geq (N_g e_T = 28\,\mu\text{s})$ in Table II and there is no white Gaussian noise [1], [2].

Fig. 13 depicts the operation process of the proposed fine STR when $\tau_1^1 = (\rho \cdot T_u/Dx = 129\ \mu\text{s})$ and $h_1^1 = -15$ dB. In Fig. 13(c), a circularly shifted pre-echo outside the GI is observed. From (13), the pre-echo appears in the region R_b, thus the corresponding STO is calculated by (20). Fig. 13(a) shows that the FFT window is changed three times in total in order $\triangle\hat{\theta}_b^{pre'} \rightarrow \triangle\hat{\theta}_a^{post} \rightarrow \triangle\hat{\theta}_b^{pre'}$. In particular, it is verified from Fig. 13(b) that the STO calculation method of (20) minimizes the amounts of ISI and ICI. Fig. 13(c) shows $|\hat{h}^{1'}|^2$ after the fine STR, which is matched with the illustration of Fig. 5(c).

Fig. 14 shows SER curves of the proposed sparse equalization and conventional equalizations as the function of the pre-echo delay (τ_1^1) when $h_1^1 = -9/-12/-15$ dB. Here, it is noticed that the FI filter is generated by (28) if the channel is identified as a single pre-echo outside the GI after the fine STR. The main objective of the FI filter is to further minimize the ISI and ICI effects. In Fig. 14, it is found that the conventional equalization without the proposed fine STR shows the error floor problem unlikely the others. This proves that the proposed fine STR can minimize effectively the effects. Furthermore, we can see that the proposed sparse equalization can improves further the SER performance compared to no sparse equalization.

VII. Conclusion

In this paper, we proposed an improved CIR-based receiver that includes the fine STR and sparse equalization for SISO and MISO transmission modes of DTV-T2 system. In these schemes, we presented the proposed CIR-based fine STR capable of resolving an ambiguity effect of CIR caused by a false coarse STO. The proposed CIR-based sparse equalization was then presented for use in a large delay spread channels. Here, it is noticed that the sparse equalization is archived through the generation of FI filter according to the sparse behavior of a channel. Finally, the simulation results of the proposed receiver were presented both in pre-echo channels causing the ambiguity effect of CIR. We showed that the proposed receiver provides a fine STO without the ISI and improves SER performance in the pre-echo within the GI. In particular, we showed that the proposed receiver is capable of minimizing the ISI and ICI effects in a single pre-echo outside the GI.

References

[1] NorDig, NorDig Unified Requirements for Integrated Receiver Decoders for Use in Cable, Satellite, Terrestrial and IP-Based Networks Jan. 2009, NorDig-T2 ver. 1.0.
[2] DTG , UHF Transmission and Reception. ver. 6.0, Mar. 2009.

[3] "Frame structure channel coding and modulation for a second generation digital terrestrial television broadcasting system (DVB-T2)," DVB Document A122, Jun. 2008.
[4] "Implementation guidelines for asecond generation digital terrestrial television broadcasting system (DVB-T2)," DVB document A133, Feb. 2009.
[5] S. Alamouti, "A simple transmit diversity technique for wireless communications," *IEEE J. Select. Areas Commun.*, vol. 16, pp. 1451–1458, Oct. 1998.
[6] B. Yang, K. B. Letaief, R. S. Cheng, and Z. Cao, "Timing recovery for OFDM transmission," *IEEE J. Select. Areas Commun.*, vol. 18, no. 11, pp. 2278–2291, Nov. 2000.
[7] M. Morelli, C.-C. J. Kuo, and M.-O. Pun, "Synchronization techniques for orthogonal frequency division multiple access (OFDMA): A tutorial review," *IEEE Proc.*, vol. 95, no. 7, pp. 1394–1427, Jul. 2007.
[8] J.-J. van de Beek, M. Sandell, and P. Borjesson, "ML estimation of time and frequency offset in OFDM systems," *IEEE Trans. Signal Process.*, vol. 45, pp. 1800–1805, 1997.
[9] A. I. Bo, G. E. Jian-Hua, and W. Yong, "Symbol synchronization technique in COFDM systems," *IEEE Trans. Broadcast.*, vol. 50, no. 1, pp. 56–62, Mar. 2004.
[10] H. Minn, V. K. Bhargava, and K. B. Letaief, "A robust timing and frequency synchronization for OFDM systems," *IEEE Trans. Wireless Commun.*, vol. 2, pp. 822–839, Jul. 2003.
[11] Y. Mostofi and D. Cox, "Mathematical analysis of the impact of timing synchronization errors on the performance of an OFDM system," *IEEE Trans. Consum.*, vol. 49, no. 4, pp. 949–957, Feb. 2006.
[12] D. C. Chang, "Effect and compensation of symbol timing offset in OFDM systems with channel interpolation," *IEEE Trans. Broadcast.*, vol. 54, no. 4, pp. 761–770, Dec. 2008.
[13] M. Speth, S. Fechtel, G. Fork, and H. Meyr, "Optimum receiver design for wireless broad-band systems using OFDM—Part I," *IEEE Trans. Commun.*, vol. 47, pp. 1668–1677, Nov. 1999.
[14] M. Speth, S. Fechtel, G. Fork, and H. Meyr, "Optimum receiver design for OFDM-based Broadband transmission. Part II: A case study," *IEEE Trans. Commun.*, vol. 49, pp. 571–578, Apr. 2001.
[15] Y. Mostofi, D. C. Cox, and A. Bahai, "Effect of frame synchronization errors on pilot-aided channel estimation in OFDM: Analysis and solution," in *In Proc. IEEE Int. Symp. Wireless Personal Multimedia Commun.*, Honolulu, USA, Oct. 2002, pp. 1309–1313.
[16] J. S. Baek and J. S. Seo, "Effective symbol timing recovery based on pilot-aided channel estimation for MISO transmission mode of DVB-T2 system," *IEEE Trans. Broadcast.*, vol. 7, no. 2, pp. 2603–2611, Jun. 2010.
[17] M. Liang and D. C. Yang, "Channel impulse response order adjustment for OFDM in SFN," in *4th Inter. Conf. WiCOM 2008*, Oct. 2008, pp. 1–4.
[18] M.-H. Hsieh and C.-H. Wei, "Channel estimation for OFDM systems based on comb-type pilot arrangement in frequency selective fading channels," *IEEE Trans. Consum.*, vol. 44, pp. 217–225, Feb. 1998.
[19] K. H. Mo, H. K. Song, and D. K. Hong, "A timing recovery for return channel of digital video broadcasting," *IEEE Trans. Consum.*, vol. 48, no. 3, pp. 624–630, Aug. 2002.
[20] I. J. Fevrier, S. B. Gelfand, and M. P. Fitz, "Reduced complexity decision feedback equalization for multipath channels with large delay spreads," *IEEE Trans. Commun.*, vol. 47, pp. 927–937, Jun. 1999.
[21] S. Ariyavisitakul, N. R. Sollenberger, and L. J. Greenstein, "Tap selectable decision-feedback equalization," *IEEE Trans. Commun.*, vol. 45, pp. 1497–1500, Dec. 1997.
[22] M. Kocic, "Sparse equalization for real-time digital underwater acoustic communications," in *In Proc. OCEANS95*, San Diego, CA, Oct. 1995, pp. 1417–1422.